Hindawi
Shock and Vibration
Volume 2019, Article ID 9616859, 13 pages
https://doi.org/10.1155/2019/9616859

Research Article

Numerical Simulation of Dynamic Damage and Stability of a Bedding Rock Slope under Blasting Load

Yekai Chen,[1] Junhao Xu,[1] Xiaohui Huo,[1] and Jinchang Wang[2]

[1]*South China University of Technology, 381 Wushan Rd., Guangzhou 510641, China*
[2]*Zhejiang University, 866 Yuhangtang Rd., Hangzhou 310058, China*

Correspondence should be addressed to Jinchang Wang; wjc501@zju.edu.cn

Received 16 April 2019; Revised 27 June 2019; Accepted 4 July 2019; Published 29 July 2019

Academic Editor: Davood Younesian

Blasting excavation of a bedding rock slope is a common problem in highway construction in mountainous areas. Accurate simulation of damage area caused by blasting excavation is of great significance for the subsequent maintenance of slopes. Based on a highway construction project in Guangdong province of China, a tensile and compressive damage model was used to simulate the whole process of blasting excavation of a typical bedding rock slope. The analysis results show that damage first appears just around the blasting hole and then develops to the both sides and the bottom of the blasting hole, and finally a large range of damage appears in the lower part of the blasting hole, and the damage depth on the right-side slope is around 2 m, which is in consistent with the scene. Besides, damage also occurs in the middle of the bedding rock mass of the slope. At the same time, the history analysis of vibration velocity also indicates that tensile failure appears on the right-side slope under the blasting hole. Therefore, the stability of the slope can be assessed by analyzing the distribution of damage factors and the vibration velocity characteristics synthetically. In addition, parameter analysis was also carried out to optimize the blasting design by controlling the blasting load so as to obtain the ideal blasting excavation effect and ensure the stability of the slope under blasting load.

1. Introduction

During the construction of highways, it is inevitable to encounter various complicated geological conditions, such as the excavation of rocky high slopes. Compared with the soil slope, the strength of the rock slope is greater and the excavation is more difficult, so blasting excavation is often required. In the dynamic response analysis of blasting excavation of the slope, there are many influencing factors: the characteristic parameters of rock, blasting, and groundwater, in which blasting is a transient process of high temperature, high pressure, and high speed, which is different from the general load. At present, the research on the stability of the high cut slope mainly focuses on the long-term safety and stability of the rock slope caused by unloading after the excavation of the rock mass [1–3]. However, the dynamic stability analysis of the slope under the action of blasting load is still in the exploration stage, and there is still a long distance before it can be applied to engineering practice. In recent years, researches on blasting excavation of high slopes mainly focused on field tests and numerical simulation. Liu et al. [4] studied the excavation blasting test of the high and steep slope of Xiaowan Hydropower Station and obtained the safety criterion of high-slope blasting. Ouyang et al. [5] analyzed the influence of blasting disturbance on the stability of slope rock mass for a convex rock slope blasting excavation project, and the safety threshold of particle vibration velocity of the rock slope was discussed and determined. Chen et al. [6] simulated the dynamic response of the rock slope under blasting load, which proved the feasibility of numerical simulation. Xiao et al. [7] carried out numerical simulation of single-hole blasting along the inclined slope with a weak interlayer and determined that the action of blasting layer splitting has zoning characteristics. Based on the Yanqing-Longqingxia Road reconstruction project, Gao et al. [8] established a finite element analysis

model of the dynamic response of the cutting slope under the action of explosion load and analyzed the impact of different blasting methods and different slope gradient designs on blasting excavation. Hu et al. [9] used a tensile and compressive damage model to simulate the blasting excavation damage effect of the 640 m high-level slope, retaining rock mass of the Xiluodu high slope. Then, the results were compared with the measured damage area obtained by the rock sound wave test, which verified the calculation model effectiveness, and comparing with the commonly used blasting damage model, the accuracy of the tensile compression model is slightly improved. Chen et al. [10] analyzed the influence of blasting excavation on water-bearing cracks in rock mass and obtained the relationship between peak vibration velocity and pore water pressure. Yan et al. [11] obtained the relationship between the peak velocity of the particle point and the depth of damage under different blasting distances by velocity vibration monitoring and damage acoustic wave monitoring. Yang et al. [12] proposed a new constitutive model for rock blasting damage caused by pulse loading of stress waves, which assumes that the brittle failure of rock during blasting is controlled by tensile strain. Li et al. [13] used numerical analysis methods to study the blasting load, rock damage characteristics, and peak particle velocity (PPV) attenuation law and obtained a simple method based on the safety threshold of rock vibration velocity to limit the damage depth of rock mass during blasting excavation. Based on the rock blasting theory of Langefors, Bastante et al. [14] established a new constitutive model for predicting the extent of rock damage caused by explosion. Hamdi et al. [15] used digital image technology to evaluate the internal microcracks of samples before and after the field explosion and determined the internal damage condition of the rock by the ratio of specific crack area to the total image area, thus deducing a general blasting damage evaluation method.

In this paper, three-dimensional numerical analysis of the blasting excavation process of a bedding rock slope was carried out by using a tensile and compressive damage plastic model. The damage occurrence and development rules of rock mass in the blasting process of the rock slope and the diffusion characteristics of blasting vibration velocity in rock mass were studied. Then, the blasting excavation effect and the stability of the rock slope were judged according to the distribution of blasting damage area and vibration velocity. Furthermore, through the parameter analysis, the design parameters of blasting excavation were optimized to ensure the blasting excavation effect and the overall stability of the rock slope.

2. Elastoplastic Damage Model of Rock Mass

The development of a rock mass blasting model can be divided into three stages: elastic stage, fracture stage, and damage stage. The damage model simulates the damage and failure process of rock mass under blasting load through damage variables and gradually becomes an important model to study the damage characteristics of rock during blasting excavation [16]. In this paper, the plastic model of tensile and compressive damage in ABAQUS is used for the numerical simulation of rock blasting, which is suitable to analyze the tensile and compressive damage of brittle materials such as rock mass. This model is a continuous, plastic-based rock damage model. It assumes that the rock mass material is mainly destroyed by tensile cracking and compression fracture, and the evolution of the yield or failure surface is controlled by two hardening variables ($\tilde{\varepsilon}_t^{pl}$ and $\tilde{\varepsilon}_c^{pl}$), which represent the tensile and compressive equivalent plastic strain, respectively. This model assumes that the uniaxial tension and compression response of the rock mass have the characteristics of plastic failure, as shown in Figure 1.

Under uniaxial tension, the stress-strain response follows the linear elastic relationship until the value of the failure stress σ_{t0} is reached, which corresponds to the generation of microcracks in the rock mass materials. In the case of uniaxial compression, the initial response is linear until the yield stress σ_{c0} is reached. The initial stress-strain response usually appears as strain hardening and then begins to show strain softening when the ultimate pressure σ_{cu} is reached.

It is assumed that the uniaxial stress-strain curve can be transformed into a relationship between stress and plastic strain. Therefore,

$$\begin{cases} \sigma_t = \sigma_t\left(\tilde{\varepsilon}_t^{pl}, \dot{\tilde{\varepsilon}}_t^{pl}, \theta, f_i\right), \\ \sigma_c = \sigma_c\left(\tilde{\varepsilon}_c^{pl}, \dot{\tilde{\varepsilon}}_c^{pl}, \theta, f_i\right), \end{cases} \tag{1}$$

where subscripts t and c represent stretching and compression, respectively; $\tilde{\varepsilon}_t^{pl}$ and $\tilde{\varepsilon}_c^{pl}$ are equivalent plastic tensile strain and compressive strain, respectively; $\dot{\varepsilon}_t^{pl}$ and $\dot{\varepsilon}_c^{pl}$ are equivalent plastic tensile strain rate and compressive strain rate, respectively; θ is temperature; and f_i ($i = 1, 2, \ldots$) are other predefined field variables.

When the specimen is unloaded from the softening section of the stress-strain relation curve, the unloading section is weakened (the slope of the curve decreases), as shown in Figure 1, which indicates that the elastic stiffness of the material is damaged (or weakened). The damage (weakening) of the elastic stiffness can be expressed by two damage variables d_t and d_c, which are assumed to be a function of plastic strain, temperature, and field variables, namely,

$$\begin{cases} d_t = d_t\left(\tilde{\varepsilon}_t^{pl}, \theta, f_i\right), & 0 \le d_t \le 1, \\ d_c = d_c\left(\tilde{\varepsilon}_c^{pl}, \theta, f_i\right), & 0 \le d_c \le 1. \end{cases} \tag{2}$$

The damage factor ranges from 0 (for nondestructive materials) to 1 (for completely damaged materials).

If E_0 is the initial (nondestructive) elastic stiffness of the material, the stress-strain relationship under uniaxial tension and compressive loads is

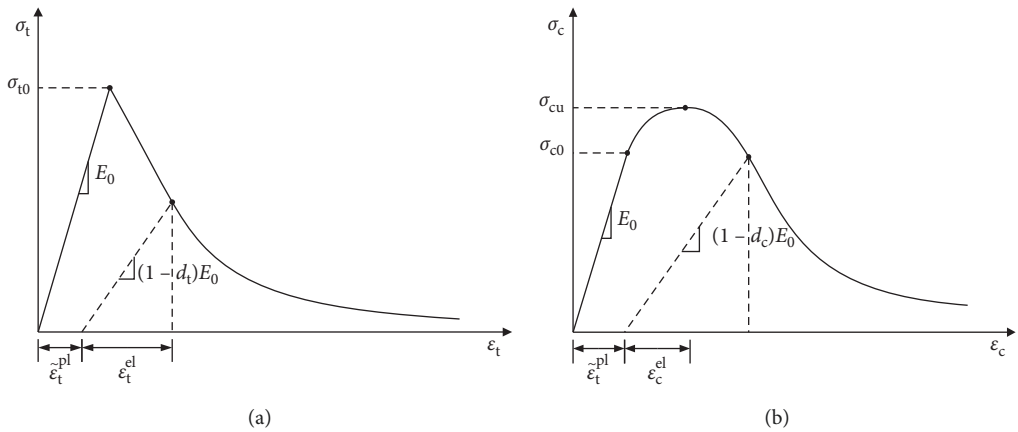

Figure 1: Stress and strain curves (a) uniaxial tensile rock mass and (b) uniaxial compression rock mass.

$$\begin{cases} \sigma_t = (1-d_t)E_0\left(\varepsilon_t - \tilde{\varepsilon}_t^{pl}\right), \\ \sigma_c = (1-d_c)E_0\left(\varepsilon_c - \tilde{\varepsilon}_c^{pl}\right). \end{cases} \tag{3}$$

The "effective" tensile and "effective" compressive stress are

$$\begin{cases} \overline{\sigma}_t = \dfrac{\sigma_t}{(1-d_t)} = E_0\left(\varepsilon_t - \tilde{\varepsilon}_t^{pl}\right), \\ \overline{\sigma}_c = \dfrac{\sigma_c}{(1-d_c)} = E_0\left(\varepsilon_c - \tilde{\varepsilon}_c^{pl}\right). \end{cases} \tag{4}$$

The effective stress determines the size of the yield (or failure) surface.

The damaged plasticity model assumes that the reduction of the elastic modulus is given in terms of a scalar degradation variable d as

$$E = (1-d)E_0, \tag{5}$$

where E_0 is the initial (undamaged) modulus of the material.

The stiffness degradation variable, d, is a function of the stress state and the uniaxial damage variables, d_t and d_c. Meanwhile, variable d is also considered as a damage factor of the material, which is used to assess the dynamic damage characteristics of a typical bedding rock slope under blasting load in the numerical analysis of this paper.

3. Numerical Model of Blasting Excavation of a Bedding Rock Slope

3.1. Description of Project and Problems. In this paper, a bedding rock slope under construction is studied, which is located beside a highway in northern Boluo County, Guangdong Province of China. The studied slope is located in the hilly area, and the terrain is rugged. The slope elevation is about 122~202 m, and the natural slope angle is about 30°. The slope has been excavated to 5th grade and 6th grade, and the outcrop is medium to microweathered granite. The cross section of the slope is shown in Figure 2, and the excavation and reinforcement design from the top of 5th grade to 8th grade are depicted in this figure. The figure shows the excavation and reinforcement design from the top of 5th grade to 8th grade. According to the distribution of rock strata, the rock layers of the slope from top to bottom are silty clay, fully weathered granite, strongly weathered granite, moderately weathered granite, and microweathered granite in sequence. It is a bedding rock slope, in which the moderately weathered granite layer is thin, and it is very close and almost parallel to the slope surface at the 6th and 7th grade slopes.

The slope was excavated by explosive blasting in the construction process. According to the site construction, blasting vibration expanded the crack surface near the location of slope blasting so that the crack surface was penetrated and the rock mass collapsed along the sloping structural surface. The collapse ranged from the 5th grade slope to the platform. The partial failure of the platform was 0.5 m wide, about 60 m in length, and the depth was about 2 m. The partial collapse location of the slope is shown in Figure 3.

Blasting excavation will cause inevitable damage to the slope, which may cause certain hidden danger to the slope in the future. How to precisely control the damaged area of the blasting slope is an urgent problem to be solved in the current blasting excavation, which is of great significance for the slope reinforcement and the landslide prediction. With the development of computer, numerical calculation has become an effective tool for blasting excavation research [17].

3.2. Numerical Analysis Model. In this paper, the blasting excavation process of the bedding rock slope introduced in Section 3.1 is chosen to be the engineering prototype (Figure 2) of the numerical analysis model. The bedding rock slope from the top of the excavated 5th grade to the 8th grade is selected as the simulation object. The finite element numerical model is shown in Figure 4. The dimension of the model is 120 m × 80 m × 2 m. The geological stratification is divided into four layers, which are silty clay, strongly

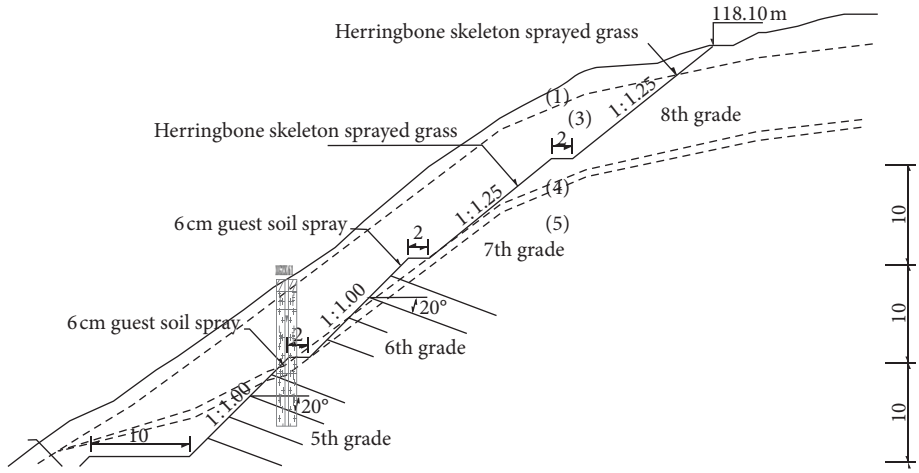

Figure 2: Distribution of slope strata. (1) Silty clay, (2) fully weathered granite, (3) strongly weathered granite, (4) moderately weathered granite, and (5) microweathered granite.

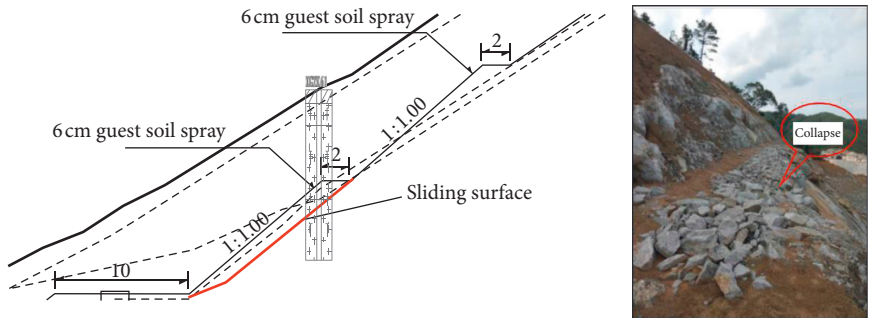

Figure 3: Local collapse of the slope caused by blasting excavation. (a) Sliding surface. (b) Collapse on-site.

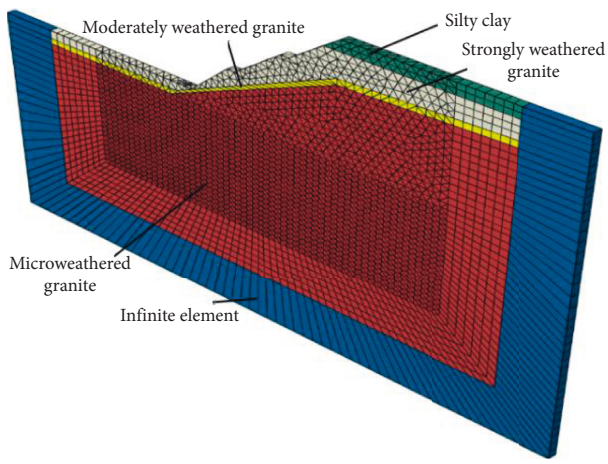

Figure 4: Finite element model of the bedding rock slope (different rocks in different colors).

weathered granite, moderately weathered granite, and microweathered granite, respectively, from top to bottom. The moderately weathered granite is relatively thin, and the dividing line is simplified from curve to broken line.

The Mohr–Coulomb model is used to simulate the silty clay layer, and the tensile and compressive damage plastic model is used to simulate the strongly weathered granite, moderately weathered granite, and lightly weathered granite.

Laboratory tests of granite with plastic damage were conducted to provide material parameters for the finite element models, as listed in Table 1. The tensile and compressive plastic damage properties of weathered granite were calibrated by the direct tensile test (DTT) and uniaxial compression test (UCT), respectively. The tensile and compressive failure stress of all kind of weathered granite is listed in Table 1.

3.3. Boundary Conditions. Due to the reflection and scattering effects of waves, the mesh boundary may reflect energy to the simulation region, which will affect the calculation results. Therefore, boundary conditions should be taken into account when solving a dynamic problem. In order to reduce the reflection of boundary on the wave, infinite elements are set on the left side, the right side, and the bottom surface to simulate the semiinfinite space of rock and soil mass, as shown in Figure 4.

3.4. Finite Element Mesh. The mesh size directly affects the accuracy and convergence of the whole model. According to

Table 1: Parameters of the rock-soil model.

Rock and soil type	Unit weight (kN/m^3)	Cohesion (kPa)	Internal friction angle (°)	Compressive strength (MPa)	Tensile strength (MPa)	Poisson's ratio	Damping ratio
Silty clay	18.0	19	18	—	—	0.3	0.03
Strongly weathered granite	21.0	31	32	10.95	0.32	0.28	0.03
Moderately weathered granite	22.0	34	34	15.19	1.07	0.25	0.03
Microweathered granite	22.5	37	35	16.50	3.56	0.21	0.03

the properties of rock mass, if Poisson's ratio is neglected, the wave velocity can be estimated as

$$c_d = \sqrt{\frac{E}{\rho}} = 4.53 \times 10^3 \text{ m/s}, \quad (6)$$

where E is the modulus of elasticity and ρ is the density of soil.

Numerical simulation shows that the span of the blasting load is relatively appropriate within 10 units of finite element because the duration of load is 0.007 s, so the length of wave propagation after the blasting load is $L = c_d \times t = 31.61$ m. Therefore, the length of each element is 3.1 m, so the preliminary mesh division is 3.1 m. Finally, according to the size of deformation, the final meshing is 2.0 m, which is more accurate.

3.5. Blasting Load

3.5.1. Blasting Position. The blasting site is located on the slope of the fifth grade, passing through three rock layers from top to bottom, namely, highly weathered granite, moderately weathered granite, and microweathered granite. The location of the blasting hole is shown in Figure 5.

3.5.2. Blasting Load. The blasting load is mainly caused by the gas expansion pressure generated by the explosion. If the coupled charge condition is adopted, the wall pressure of the blasting hole is

$$p_h = \frac{\rho_0 D^2}{2(k+1)}. \quad (7)$$

If the uncoupled charge condition is adopted, the wall pressure of the blasting hole is

$$p_h = \frac{\rho_0 D^2}{2(k+1)} \left(\frac{d_c}{d_h}\right)^{2k}, \quad (8)$$

where p_h is the hole wall pressure (MPa); ρ_0 is the explosive density (kg/m^3); D is the explosive detonation velocity (m/s); k is the isentropic index, value 3.0; and d_c and d_h are the charge diameter and hole diameter (mm), respectively.

Since the explosive blasting is a complex instantaneous process, in order to facilitate the analysis, the blasting load is simplified as follows: the time history curve of the blasting load is simplified as a triangle, that is, the load rises linearly to the highest load in the first 1 ms before unloading, and then the linear drop of the pressure lasts 6 ms [18, 19].

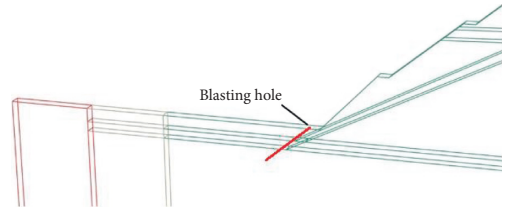

Figure 5: Position of the blasting hole.

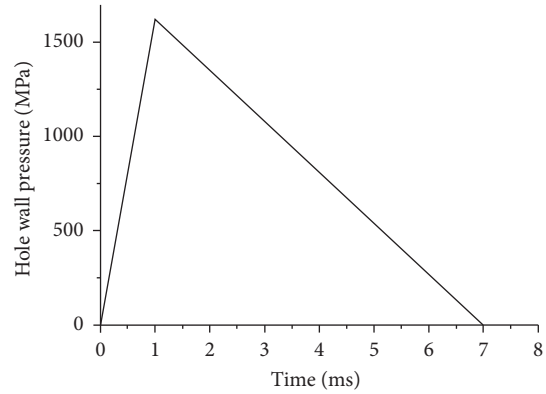

Figure 6: Time history diagram of equivalent load (with a peak value of 1620 MPa).

In this paper, the numerical analysis of the corresponding field for coupling charging conditions of the blasting scheme is performed. According to field data, the diameter of the blasting hole is 80 mm, the inclination angle of the drilling hole is 40°, the hole spacing is 2.0 m, the detonation velocity is 3600 m/s, and the explosive density is 1000 kg/m^3. Thus, the peak blasting load $p_h = 1620$ MPa can be calculated by formula (7), and the change of the blasting load along time is shown in Figure 6.

4. Results and Discussion

The distribution and development law of damage factors in rock mass under blasting load was analyzed, as well as the diffusion characteristics of rock mass vibration velocity. The blasting mechanism of the rock mass slope and the influence of blasting excavation on the stability of the rock mass slope were analyzed and discussed in combination with the practical project corresponding to the numerical model.

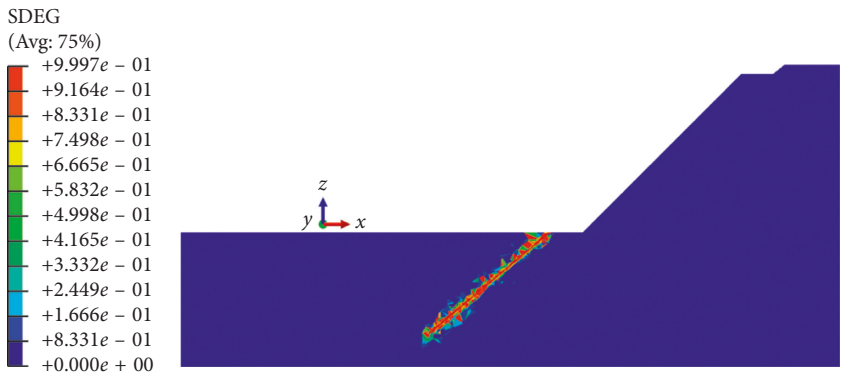

(a)

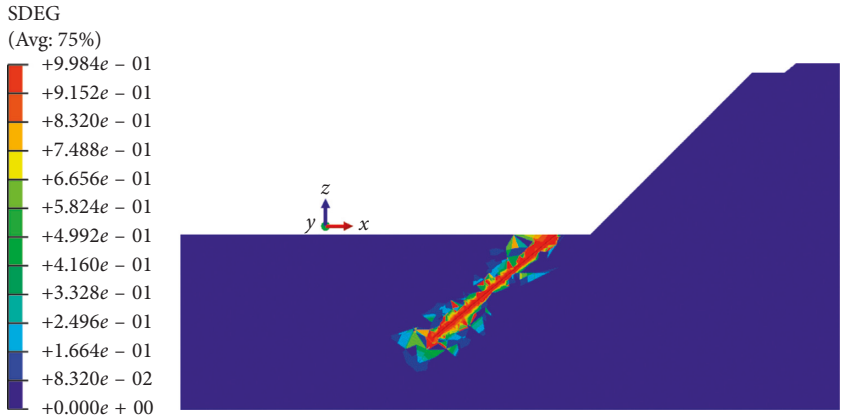

(b)

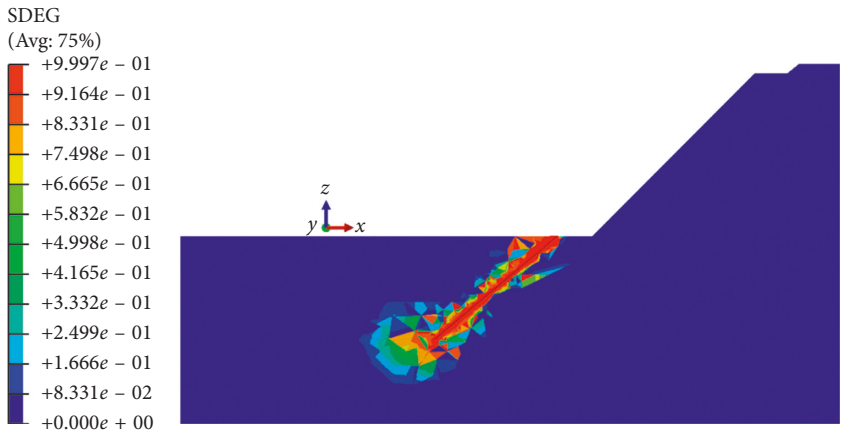

(c)

Figure 7: Continued.

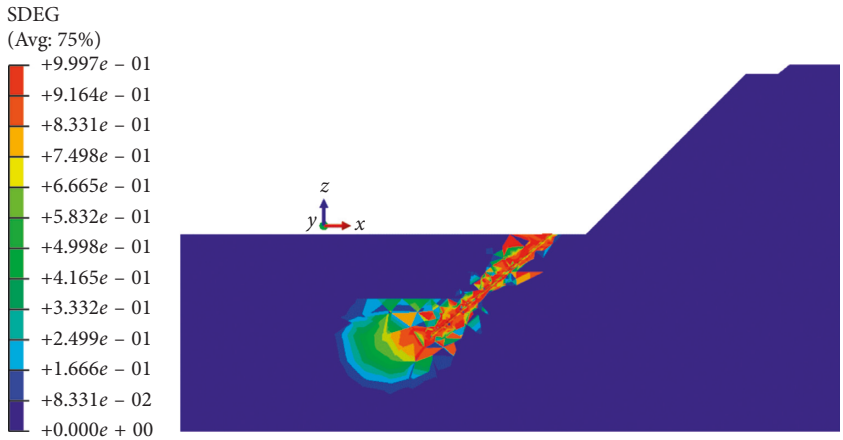

(d)

Figure 7: Time history contours of the slope damage factors after blasting at (a) 1 ms, (b) 3 ms, (c) 5 ms, and (d) 7 ms.

4.1. Damage Characteristics of Rock Mass. According to the numerical simulation of the blasting process, the change and development process of damage factors of the slope rock mass during the blasting process can be obtained. The distribution of damage factors of the slope rock mass at different times is shown in Figure 7, where the output variable "SDEG" is the stiffness degradation of material, namely, the damage factor of the slope rock mass. After blasting for 1 ms (Figure 7(a)), damage begins to occur around the blasting hole. The damage area is small, but the damage factor variable is close to 1, forming a fracture zone. After 3 ms (Figure 7(b)), the damage range of the rock mass extends at the both sides of the blasting hole, and the fracture area increases gradually. After 5 ms (Figure 7(c)), the damage range of the slope rock mass continues to spread around and the damage of the moderately weathered granite is aggravated. Meanwhile, the damage rate at both ends of the blasting hole is faster, especially at the bottom of the blasting hole, and the rock mass damage is the most serious. After 7 ms (Figure 7(d)), the damage range of the rock mass at the bottom of the blasting hole continues to expand, forming a spherical damage area. The damage depth on the right-side slope is around 2 m, which is in consistent with the scene. The damage area is inclined to the left side of the borehole, achieving the effect of blasting excavation. On the right side of the blasting hole, the damage range of the rock mass is not obviously expanded, but the damage factor increases with the increase of blasting time. After 7 ms, the damage factor of the rock mass on the right side of the blasting hole basically reaches 0.8~0.9, which will adversely affect the stability of rock slopes.

According to the numerical analysis of the damage evolution of the rock mass in the blasting process, it can be seen that the blasting excavation in the bedding slope will cause damage to the weathered granite, and the damage in the lower part of the blasting hole will be serious, causing the crack between rock layers to expand and cause the collapse. The results of the numerical analysis are in good agreement with the on-site postblasting condition of the actual slope.

Table 2: Rock damage effect under different V_{PP} [20].

V_{PP} (m/s)	Rock mass damage effect
(0, 0.25)	Complete rock will not crack
(0.25, 0.635)	Slight tensile cracking
(0.635, 2.54)	Severe tensile cracks and some radial cracks
(2.54, +∞)	The rock mass is completely broken

4.2. Vibration Velocity Analysis. The study of Bauer and Calder [20] shows that the damage range of the slope is closely related to the magnitude of blasting vibration velocity. Table 2 shows the correspondence between the vibration velocity (V_{pp}) and the rock damage effect.

In this paper, the time history of vibration velocity of the slope after blasting is numerically analyzed. Figure 8 is the contours of vibration velocity distribution of slope rock mass at different blasting moments. According to Table 2, only when the vibration velocity is above 0.25 m/s, cracks begin to appear in the rock mass till the rock mass is broken. Therefore, 0.25 m/s or more is selected from the vibration velocity contours. When the vibration velocity is higher than 2.54 m/s, the color of the contours is set as grayish white, as shown in Figure 8. As can be seen from the velocity distribution contours, the vibration velocity of the slope surface can reach 10.71 m/s at 1 ms of the beginning of the blasting, and the diffusion decreases toward the periphery. At 1.5 ms, the vibration velocity is transmitted to the fifth platform on the right side and the inside of the slope. Its internal vibration velocity is from 0.44 to 0.63 m/s. At 2 ms, the vibration velocity inside the right-side slope was continuously transferred to the interior, and the range was continuously expanded. At 3 ms, the vibration velocity of the right-side slope decreases, and finally at 7 ms, the vibration velocity decreases as a whole and the range of the right side of the slope decreases. From the time history analysis of the blasting and by referring to Table 2, it can be concluded that when the blasting load is maximum at 1 ms, the surface vibration velocity of the blasting hole reaches the maximum value, and a fracture area is formed near the blasting hole. During 1 to 2 ms of the blasting, the vibration velocity of the

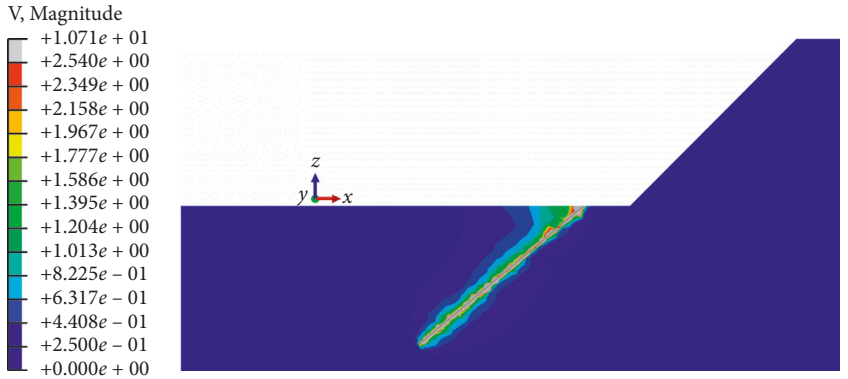

(a)

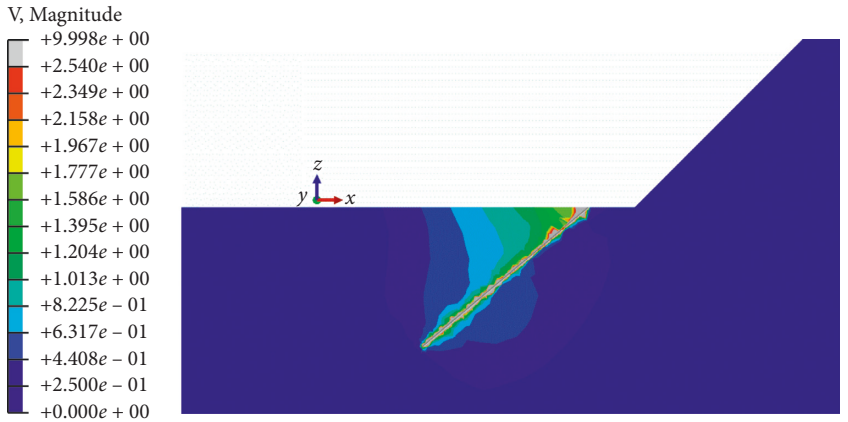

(b)

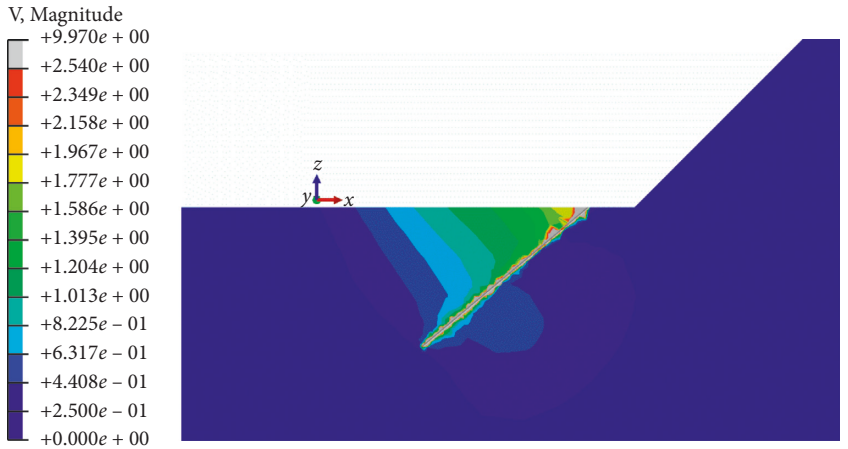

(c)

Figure 8: Continued.

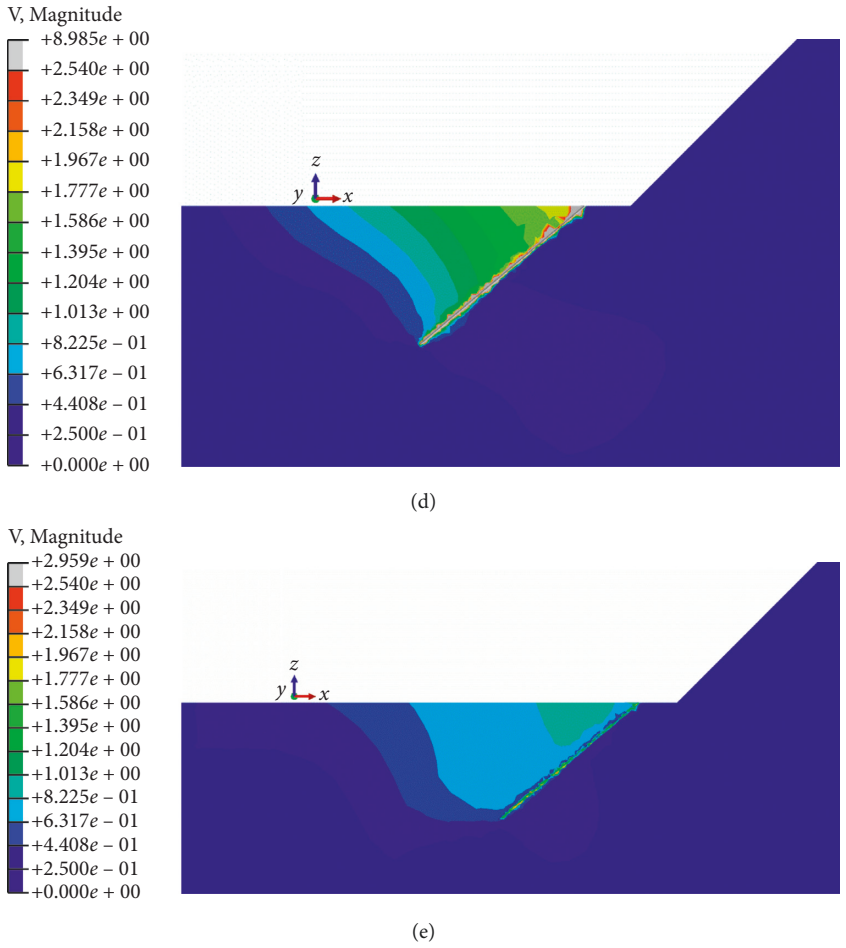

Figure 8: Time history contours of slope vibration velocity after blasting at (a) 1 ms, (b) 1.5 ms, (c) 2 ms, (d) 3 ms, and (e) 7 ms.

lower part of the blasting hole on the right side of the slope reaches 0.44 to 0.63 m/s, and tensile cracking occurs.

Based on the damage evolution of rock mass and the characteristics of blasting velocity transmission and distribution under blasting load, it can be seen that under the action of blasting vibration, in addition to the blasting excavation effect, blasting damage and vibration velocity of slope rock mass will also develop towards the deep slope. If the rock mass slope itself has a crack surface, the cracks caused by the blasting damage will disturb and increase the existing crack surface and eventually cause the crack surface to be penetrated and the rock mass to collapse along the downdip structure surface.

5. Optimization Analysis of Blasting Design

From the above analysis, it can be seen that blasting excavation under coupled charging condition disturbs the existing crack surface of slope rock mass due to blasting vibration, which makes the crack surface to pass through the whole rock mass, together with the damage of rock mass itself, and eventually leads to slope collapse. In this section, according to blasting theory and equations (7) and (8), different blasting numerical analyses are carried out. Measures, including changing explosive density, changing coupling charge conditions into uncoupling charge conditions, and reducing the blasting load are taken into consideration, aim to optimize the existing blasting design and achieve the purpose of preventing the rock slope from collapsing during the blasting.

Under the condition of uncoupled charge, the charge diameter is 70 mm, and the other conditions are the same as the coupled charge conditions. According to equation (8), the blasting load is 727.1 MPa, and then the blasting analysis is performed. The analysis results of the blasting vibration velocity are shown in Figure 9.

As shown in Figure 9, when the charging condition becomes uncoupled, the maximum vibration velocity becomes 3.67 m/s at 2 ms, which is equivalent to 37% of the maximum vibration velocity under the coupled charge condition, and the slope is almost not affected by any damage on the right side. The vibration velocity of the left-side slope is 0.25~0.63 m/s, and the degree of damage is only a slight tensile fracture.

It can be seen that changing the charging condition can significantly reduce the blasting load. Although the right-side slope is not affected, the left-side slope cannot achieve

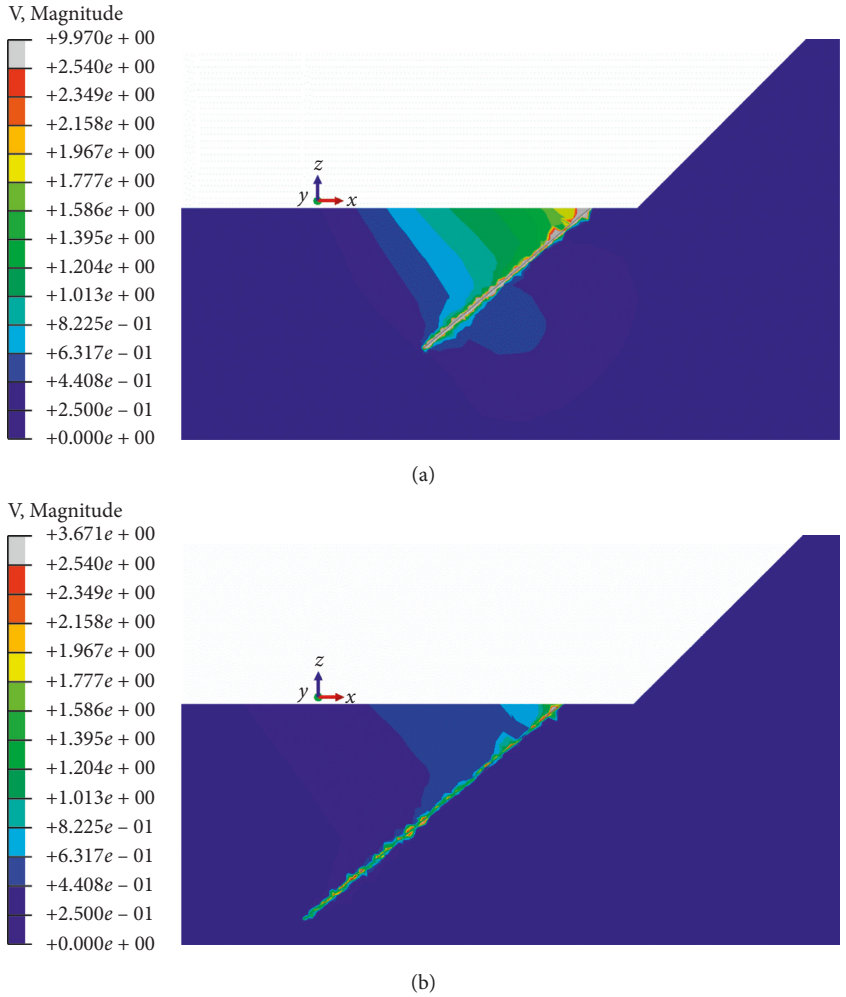

Figure 9: Contours of blasting vibration velocity at 2 ms under different charging conditions. Blasting load: (a) 1620 MPa and (b) 727.1 MPa.

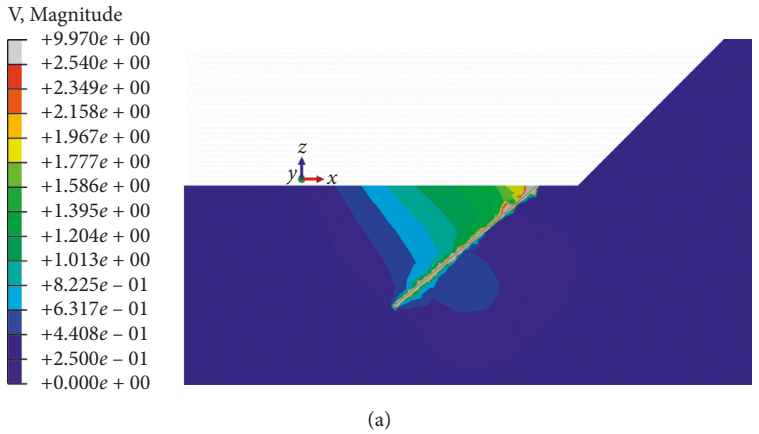

Figure 10: Continued.

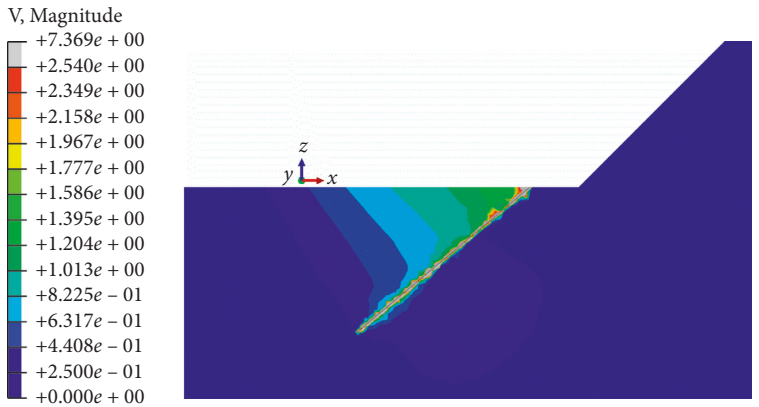

(b)

Figure 10: Contours of vibration velocity of 2 ms blasting under different explosive densities. Blasting load: (a) 1620 MPa and (b) 1296 MPa.

an ideal blasting effect (the vibration velocity of the left-side slope reaches 0.635 m/s or more). Therefore, changing the charging conditions is not recommended.

If charging conditions remain the same, changing the density of explosive results in slight reduction in the blasting load, that is, if the density of explosive is changed from 1000 kg/m^3 to 800 kg/m^3, the blasting load is 1296 MPa, and then the blasting analysis is carried out and the analysis results are shown in Figure 10. It can be seen form Figure 10 that the range of the vibration velocity is reduced after the density of explosives is reduced, and the vibration velocity of the right-side slope is mostly around 0.25 m/s, which is reduced by 60%. Besides, its damage is reduced significantly as well. Therefore, the right-side slope is safer when the density of explosive is reduced to 800 kg/m^3. Although the maximum vibration velocity on the left side is reduced, the blasting excavation effect of the left-side slope can still be achieved.

In order to investigate the relationship between the magnitudes of blasting load and the maximum vibration velocity, models with different blasting loads are calculated. Figure 11 is the numerical result of the maximum vibration velocity at 1 ms under different blasting loads, and Figure 12 is the attenuation curve of the maximum vibration velocity under different blasting loads within 1~3 ms. It can be seen from Figure 11 that the maximum vibration velocity increases linearly with the increase of blasting load at 1 ms. For every 100 MPa increase in the blasting load, the maximum vibration velocity increases by about 0.75 m/s. As shown in Figure 12, under different blasting loads, the maximum vibration velocity decreases with time. The maximum vibration speed per second is reduced by 1 m/s, and the attenuation rate is almost unaffected by the magnitude of the blasting load.

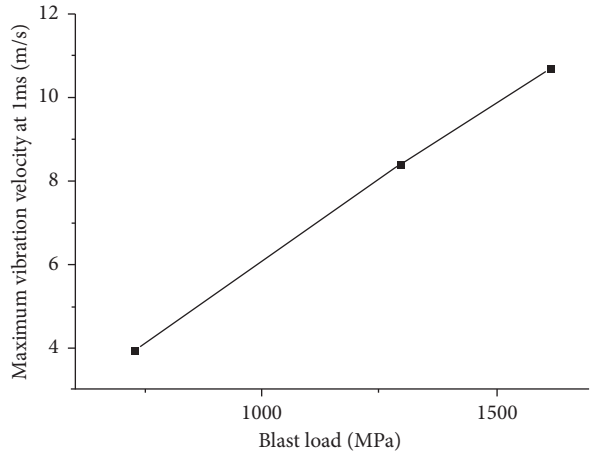

Figure 11: Maximum vibration velocity at 1 ms under different blasting loads.

6. Conclusion

In this paper, the whole process of a typical rock slope blasting excavation is simulated by using a plastic model of tensile and compressive damage, and the slope stability is assessed by analyzing the damage factors and vibration velocity characteristics synthetically. The main conclusions of this study are as follows:

(1) According to the numerical simulation results of this typical rock slope, when the blasting load is 1620 MPa, the degree of slope damage increases with time, and a broken zone will form around the blasting hole. The moderately weathered granite in the bedding strata will be damaged, and the damage factor is between 0.8 and 0.9, indicating that the moderately weathered granite is more likely to be damaged.

(2) The influence range of blasting can be obtained by analyzing the diffusion characteristics of vibration velocity. According to the time history analysis of vibration velocity, the rock mass on the right side of the slope will suffer from tensile fracture.

(3) Blasting load can greatly be reduced by changing the charging conditions, but changing the explosive density can only slightly reduce the blasting load. When the charging condition is reduced from 1620 MPa to 727.1 MPa, the blasting effect of the left-

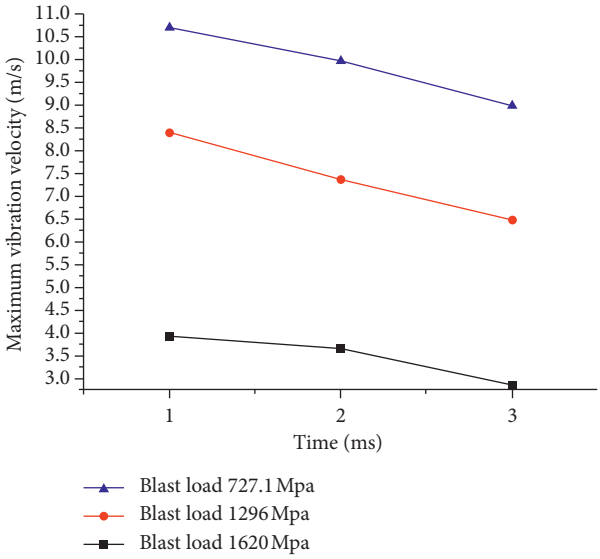

Figure 12: Maximum vibration velocity attenuation under different blasting loads within 1~3 ms.

side slope is not ideal, although the right-side slope will not collapse. By changing the explosive density and setting the blasting load to 1296 MPa, the right-side slope is relatively safe, and an ideal blasting effect is formed on the left-side slope.

(4) The maximum vibration velocity increases linearly with the increase of blasting load, but the attenuation rate is almost unaffected by the magnitude of blasting load. Therefore, when high-intensity explosives are applied in engineering, the vibration will have a long-term influence on the slope.

Data Availability

The data used to support the findings of this study are available from the corresponding author upon request.

Conflicts of Interest

The authors declare that they have no conflicts of interest.

Acknowledgments

The research was supported by the Natural Science Foundation of Guangdong Province (no. 2018A0303130150) and Science and Technology Project of Zhejinag Provincial Department of Transportation (no. 2014H27).

References

[1] Z. H. Yuan, Y. F. Liu, and H. R. Fu, "Finite element analysis of slope stress and stability under different excavation modes," *People of the Pearl River*, vol. 38, no. 8, pp. 59–63, 2017.

[2] N. W. Xu, B. Li, and F. Dai, "Stability analysis of bedding rock slope excavation based on microseismic monitoring," *Journal of Rock Mechanics and Engineering*, vol. 35, no. 10, pp. 2089–2097, 2016.

[3] X. Q. Hou and S. T. Tian, "Stability analysis of high slope excavation and reinforcement based on midas/GTS," *The Subgrade Engineering*, vol. 12, no. 6, pp. 178–181, 2013.

[4] M. S. Liu, C. Q. Wu, and Z. Y. Zhang, "Experimental study on safety criterion of blasting vibration of high slope of xiaowan hydropower station," *Journal of Yangtze River Scientific Research Institute*, vol. 31, no. 1, pp. 40–43, 2007.

[5] J. H. Ouyang, L. B. Li, and L. Wu, "Monitoring and analysis of blasting vibration of rock convex slope mass," *Blasting*, vol. 32, no. 1, pp. 54–56, 2015.

[6] Z. J. Chen, Z. Y. Zhu, and X. H. Zhou, "Study on dynamic response of rock slope under blasting load by FLAC (3D) simulation," *Blasting*, vol. 28, no. 4, pp. 8–13, 2005.

[7] Z. X. Xiao, X. B. Guo, and J. C. Zhang, "Numerical simulation and experimental study on blasting crack effect of inclined slope with weak interlayer," *Rock and Soil Mechanics*, vol. 30, no. 1, pp. 15–18, 2009.

[8] W. X. Gao, H. Y. Liu, and H. Y. Liu, "Impact analysis of blasting excavation on the stability of high slope of cutting," *Journal of Rock Mechanics and Engineering*, vol. 29, no. 1, pp. 2982–2987, 2010.

[9] Y. G. Hu, W. B. Lu, and X. H. Jin, "Numerical simulation of dynamical damage of blasting in excavation of high rock slope," *Journal of Rock Mechanics and Engineering*, vol. 31, no. 11, pp. 2204–2213, 2012.

[10] M. Chen, T. Y. Guo, and W. B. Lu, "The perturbation mechanism of blasting excavation on crack growth of slope rock mass," *Journal of Rock Mechanics and Engineering*, vol. 34, no. 7, pp. 1307–1314, 2015.

[11] P. Yan, Y. J. Zou, and W. B. Lu, "Prediction of damage area of rock slope excavation based on blasting vibration monitoring," *Journal of Rock Mechanics and Engineering*, vol. 35, no. 3, pp. 538–548, 2016.

[12] R. Yang, W. F. Bawden, and P. D. Katsabanis, "A new constitutive model for blast damage," *International Journal of Rock Mechanics and Mining Sciences and Geomechanics Abstracts*, vol. 33, no. 3, 1996.

[13] H. B. Li, X. Xia, J. C. Li, J. Zhao, B. Liu, and Y. Liu, "Rock damage control in bedrock blasting excavation for a nuclear power plant," *International Journal of Rock Mechanics and Mining Sciences*, vol. 48, no. 2, pp. 210–218, 2011.

[14] F. G. Bastante, L. Alejano, and J. González-Cao, "Predicting the extent of blast-induced damage in rock masses," *International Journal of Rock Mechanics and Mining Sciences*, vol. 56, pp. 44–53, 2012.

[15] E. Hamdi, N. B. Romdhane, and J. M. Le Cléac'h, "A tensile damage model for rocks: application to blast induced damage assessment," *Computers and Geotechnics*, vol. 38, no. 2, pp. 133–141, 2011.

[16] X. Xia, J. R. Li, and H. B. Li, "Damage characteristics of rock mass excavated by blasting at guangdong lingao nuclear power plant," *Journal of Rock Mechanics and Engineering*, vol. 48, no. 12, pp. 2510–2516, 2007.

[17] N. Li, "Numerical simulation and application of blasting load," *Journal of Rock Mechanics and Engineering*, vol. 35, no. 4, pp. 357–364, 1994.

[18] H. T. Xu, W. B. Lu, and X. H. Zhou, "Equivalent application method of blasting load in dynamic finite element simulation of blasting vibration field," *Journal of Wuhan University*, vol. 9, no. 1, pp. 67–71, 2008.

[19] Y. C. Zhang, G. H. Yang, and P. Liu, "Study on equivalent application method of blasting load in numerical calculation,"

Journal of Underground Space and Engineering, vol. 8, no. 1, pp. 56–64, 2012.

[20] A. Bauer and P. N. Calder, *Open Pit and Blast Seminar*, Mining Engineering Department, Queens University, Kingston, Ontario, Canada, 1978.